J. Fluid Mech. (2023), *vol*. 960, R2, doi:10.1017/jfm.2023.195

Backscatter of scalar variance in turbulent premixed flames

V.A. Sabelnikov[1,2], A.N. Lipatnikov[3,†], N.V. Nikitin[4], F.E. Hernández Pérez[5] and H.G. Im[5]

[1]ONERA - The French Aerospace Lab., F-91761 Palaiseau, France

[2]Central Aerohydrodynamic Institute (TsAGI), 140180 Zhukovsky, Moscow Region, Russian Federation

[3]Department of Mechanics and Maritime Sciences, Chalmers University of Technology, Göteborg, 412 96, Sweden

[4]Institute of Mechanics, Lomonosov Moscow State University, 119991 Moscow, Russian Federation

[5]Clean Combustion Research Center, King Abdullah University of Science and Technology, Thuwal 23955-6900, Saudi Arabia

(Received 24 October 2022; revised 16 December 2022; accepted 3 March 2023)

To explore the direction of inter-scale transfer of scalar variance between subgrid scale (SGS) and resolved scalar fields, direct numerical simulation data obtained earlier from two complex-chemistry lean hydrogen–air flames are analysed by applying Helmholtz–Hodge decomposition (HHD) to the simulated velocity fields. Computed results show backscatter of scalar (combustion progress variable c) variance, i.e. its transfer from SGS to resolved scales, even in a highly turbulent flame characterized by a unity-order Damköhler number and a ratio of Kolmogorov length scale to thermal laminar flame thickness as low as 0.05. Analysis of scalar fluxes associated with the solenoidal and potential velocity fields yielded by HHD shows that the documented backscatter stems primarily from the potential velocity perturbations generated due to dilatation in instantaneous local flames, with the backscatter being substantially promoted by a close alignment of the spatial gradient of mean scalar progress variable and the potential-velocity contribution to the local SGS scalar flux. The alignment is associated with the fact that combustion-induced thermal expansion increases local velocity in the direction of ∇c. These results call for development of SGS models capable of predicting backscatter of scalar variance in turbulent flames in large eddy simulations.

Key words: turbulent reacting flows

† Email address for correspondence: lipatn@chalmers.se

1. Introduction

Since fluid motion on large and intermediate scales is directly resolved in a large eddy simulation (LES) (Meneveau 2000; Lesieur, Metais & Comte 2005; Sagaut 2006), the LES framework is often considered to be the most appropriate for computational fluid dynamics (CFD) research on turbulent flows of practical relevance. However, since LES deals with velocity and scalar fields that are averaged over scales smaller than a filter size, subgrid-scale (SGS) motion is not resolved, but filtered out. Accordingly, both characteristics of this motion and its influence on the resolved fields must be modelled, with existing SGS models being challenged by specific phenomena.

For instance, according to the classical theory of locally homogeneous and isotropic turbulence in incompressible flows (Kolmogorov 1941; Monin & Yaglom 1975; Frisch 1995), both turbulent kinetic energy and mixture non-uniformities are transferred (on average) from large scales, where the energy and non-uniformities are generated, to small scales via the turbulence cascade (Richardson 1922) and are dissipated due to molecular viscosity and diffusion, respectively, at the smallest scales. However, an instantaneous local SGS energy flux obtained by filtering a turbulent velocity field fluctuates randomly and may be in the opposite direction of the mean energy flux (Leslie & Quarini 1979; Piomelli *et al.* 1991; Borue & Orszag 1998; Cerutti & Meneveau 1998). This phenomenon is known as backscatter of kinetic energy. A similar phenomenon has also been discussed in the literature of turbulent mixing (Jiménez, Valiño & Dopazo 2001; Marstorp, Brethouwer & Johansson 2007).

While the classical forward cascade statistically overwhelms backscatter in many turbulent flows (Piomelli *et al.* 1991; Jiménez *et al.* 2001; Kobayashi 2005; Marstorp *et al.* 2007), there are flows where backscatter definitely plays an important role and inverse cascade (i.e. transfer of kinetic energy or mixture non-uniformities from smaller to larger scales) can be statistically significant. As far as mixing in a non-reacting turbulent flow is concerned, three different physical scenarios are discussed in detail in a recent review article by Alexakis & Biferale (2018). These are (i) a passive scalar in incompressible turbulence, with the forward cascade dominating in this case, (ii) a passive scalar in compressible turbulence, with cascade being reversed at a sufficiently high degree of compressibility (Chertkov, Kolokolov & Vergassola 1998; Gawedzki & Vergassola 2000), and (iii) an active scalar, which affects the flow (e.g. temperature differences yield buoyancy forces). As concluded by Alexakis & Biferale (2018, p. 70), 'it is not possible to make any general conclusions about' cascade direction in case (iii). The direction depends on details such as length scales associated with scalar injection and significant influence of the scalar on the flow.

Both scenarios (ii) and (iii) are relevant to premixed turbulent flames, where heat release, density variations, dilatation and chemical reactions are confined to spatial scales, which are on the order of laminar flame thickness, and, thus, are substantially smaller than scales of large turbulent eddies, but are often larger than or comparable with Kolmogorov length scale. Therefore, in many premixed turbulent flames, active scalar fields evolve in a highly compressible flow (e.g. mean dilatation is positive, contrary to a typical non-reacting compressible flow, and is sufficiently large when compared with velocity gradients in the incoming turbulence), with injection of kinetic energy and mixture non-uniformities occurring at small scales and being well correlated (confined to the same zones). Accordingly, the phenomenon of backscatter of SGS kinetic energy in flames has received extensive attention over the past years (Kolla *et al.* 2014; Ranjan *et al.* 2016; Towery *et al.* 2016; O'Brien *et al.* 2017; Kim *et al.* 2018; Ranjan & Menon 2018; Ahmed, Chakraborty & Klein 2019; Kazbekov & Steinberg 2021, 2023; MacArt & Mueller 2021;

Datta, Mathew & Hemchandra 2022; Qian *et al.* 2022). On the contrary, backscatter of SGS scalar variance in turbulent flames has rarely been explored (Ranjan *et al.* 2016), in spite of the fact that, as noted in the next section, this phenomenon is closely linked with SGS counter-gradient scalar transport, which is often addressed in LES of premixed turbulent combustion (Boger *et al.* 1998; Weller *et al.* 1998; Tullis & Cant 2002; Richard *et al.* 2007; Pfadler *et al.* 2009; Lecocq *et al.* 2010; Klein, Chakraborty & Gao 2016; Klein *et al.* 2018).

It is noted that backscatter of SGS scalar variance is of importance not only for LES of turbulent mixing and combustion, but also for general understanding of physical mechanisms of flame-turbulence interaction. Indeed, following the pioneering work by Damköhler (1940), the influence of intense small-scale turbulence on a premixed flame is commonly reduced to turbulent mixing (Sabelnikov, Yu & Lipatnikov 2019; Sabelnikov & Lipatnikov 2021). However, under conditions associated with backscatter of SGS scalar variance, such a simplification may not be sufficient and the influence of combustion on scalar fluctuation cascade should also be taken into account.

Accordingly, the present communication aims at exploring the physics of combustion-induced backscatter of SGS scalar variance by investigating not only scalar transport by the entire turbulent velocity fields obtained in earlier direct numerical simulations (DNS), but also separate contributions to the scalar transport from solenoidal and potential velocity fields yielded by Helmholtz–Hodge decomposition (HHD) (Chorin & Marsden 1993) of the entire velocity fields. In the next section, mathematical background is summarized. The DNS attributes and numerical diagnostics are addressed in § 3. Subsequently, the obtained results are reported and discussed in § 4, followed by conclusions.

2. Background

A common practice of premixed turbulent combustion modelling consists in characterizing mixture state in a flame with a single scalar quantity c, which monotonically varies from zero in fresh reactants to unity in equilibrium combustion products and is known as the combustion progress variable (Bilger *et al.* 2005; Poinsot & Veynante 2005). Starting from the continuity equation and the following standard transport equation for c,

$$\rho\frac{\partial c}{\partial t}+\rho\boldsymbol{u}\cdot\boldsymbol{\nabla}c+\boldsymbol{\nabla}\cdot\boldsymbol{J}=\rho\dot{\omega}, \tag{2.1}$$

one can easily arrive at the following well-known transport equations for filtered (resolved) combustion progress variable $\tilde{c}$,

$$\bar{\rho}\frac{\partial\tilde{c}}{\partial t}+\bar{\rho}\tilde{\boldsymbol{u}}\cdot\boldsymbol{\nabla}\tilde{c}+\boldsymbol{\nabla}\cdot\bar{\boldsymbol{J}}=\bar{\rho}\tilde{\dot{\omega}}-\boldsymbol{\nabla}\cdot\left(\bar{\rho}\tilde{\boldsymbol{f}}\right) \tag{2.2}$$

and for filtered 'scalar energy' $\tilde{c}^2$,

$$\bar{\rho}\frac{\partial\tilde{c}^2}{\partial t}+\bar{\rho}\tilde{\boldsymbol{u}}\cdot\boldsymbol{\nabla}\tilde{c}^2+2\boldsymbol{\nabla}\cdot\left(\bar{\rho}\tilde{c}\tilde{\boldsymbol{f}}\right)=-G+2\tilde{c}\bar{\rho}\tilde{\dot{\omega}}-2\tilde{c}\boldsymbol{\nabla}\cdot\bar{\boldsymbol{J}}. \tag{2.3}$$

Here, $\bar{q}$ and $\tilde{q}\equiv\overline{\rho q}/\bar{\rho}$ designate filtered and Favre-filtered, respectively, values of the quantity q; t is time; ρ is density; $\boldsymbol{u}$ is flow velocity vector; $\boldsymbol{J}$ is molecular flux of c; $\dot{\omega}$ is rate of product creation; $\tilde{\boldsymbol{f}}=\widetilde{\boldsymbol{u}c}-\tilde{\boldsymbol{u}}\tilde{c}$ is SGS flux of c; and $G\equiv-2\bar{\rho}\tilde{\boldsymbol{f}}\cdot\boldsymbol{\nabla}\tilde{c}$ describes inter-scale flux of the scalar energy from resolved to subgrid scales (if $G>0$) or in reverse direction (if $G<0$). Thus, counter-gradient SGS scalar transport, i.e. a positive product

of the vectors $\tilde{\boldsymbol{f}}$ and $\boldsymbol{\nabla}\tilde{c}$, is a necessary condition for backscatter of SGS scalar variance. Note that (i) a transport equation for SGS scalar variance $\sigma_c \equiv \widetilde{c^2} - \tilde{c}^2$ involves the same term G, but with the opposite sign.

The focus of the present study is placed on the physics of the influence of combustion on the inter-scale flux G and, in particular, on its sign. For this purpose, it is essential to split the velocity field into potential and solenoidal components, because the former (latter) component does (does not, respectively) involve combustion-induced dilatation. Accordingly, HHD has been applied to the velocity fields, i.e.

$$\boldsymbol{u}(\boldsymbol{x}, t) = \boldsymbol{u}_s(\boldsymbol{x}, t) + \boldsymbol{u}_p(\boldsymbol{x}, t); \quad \boldsymbol{\nabla} \cdot \boldsymbol{u}_s = 0; \quad \boldsymbol{\nabla} \times \boldsymbol{u}_p = 0. \tag{2.4a–c}$$

The solenoidal velocity $\boldsymbol{u}_s(\boldsymbol{x}, t)$ is divergence-free and arises due to shear and a rigid-body rotation. The potential velocity $\boldsymbol{u}_p(\boldsymbol{x}, t)$ is curl-free and stems from dilatation due to thermal expansion. HHD offers the opportunity to directly explore potential motion due to thermal expansion and investigate the influence of this motion on the scalar cascade.

3. DNS attributes

Since simulations whose data are analysed in the present paper were already discussed earlier (Im *et al.* 2016; Uranakara *et al.* 2016; Wacks *et al.* 2016; Klein *et al.* 2018; Manias *et al.* 2019; Klein *et al.* 2020; Lipatnikov *et al.* 2020, 2021; Sabelnikov *et al.* 2021*c*, 2022*a*,*b*), only a brief summary of the DNS attributes is given below.

Unconfined statistically one-dimensional and planar, lean (the equivalence ratio $\Phi = 0.7$) hydrogen–air turbulent flames were studied by (i) adopting a detailed (9 species, 23 reversible reactions) chemical mechanism (Burke *et al.* 2012) with the mixture-averaged transport model and (ii) numerically solving unsteady three-dimensional governing equations, written in compressible form. Note that while differential diffusion effects are well known to be highly pronounced in very lean hydrogen–air flames and to significantly increase turbulent burning velocity, as reviewed elsewhere (Lipatnikov & Chomiak 2005), differential diffusion was shown (Chen & Im 2000; Im & Chen 2002) to weakly affect a mean bulk burning rate at $\Phi = 0.7$ used in the present study.

Along the flame propagation direction, inflow and outflow characteristic boundary conditions were set. Other boundaries were periodic. Divergence-free, isotropic, homogeneous turbulent velocity field was generated in a box using a pseudo spectral method (Rogallo 1981) and adopting the Passot–Pouquet spectrum (Passot & Pouquet 1987). Subsequently, the field was injected through the left boundary and decayed along the mean flow direction (x-axis). With the intention to explore corrugated flamelet and thickened flame combustion regimes (Im *et al.* 2016), the spectra were set using the same length scale $L_T = 5\,\mathrm{mm}$ of the most energetic eddies, but two different r.m.s. velocities $u_0' = 0.95$ and $6.8\,\mathrm{m\,s^{-1}}$ in cases A and B, respectively. The turbulent Reynolds number $Re_T = u_0' L_T/\nu_u = 227$ and 1623, respectively, where ν_u is the kinematic viscosity of unburned gas. Since the injected turbulent velocity field evolved along the x-direction (Sabelnikov *et al.* 2022*b*, figure 1), the flames interacted with turbulence whose characteristics, e.g. the r.m.s. velocity and integral length scale reported in table 1, depended on, but differed from u_0' and L_T, respectively, with the difference magnitude being case-dependent.

Major characteristics of two investigated cases are reported in table 1, where the laminar flame speed $S_L = 1.36\,\mathrm{m\,s^{-1}}$ and thickness $\delta_L = (T_b - T_u)/\max\{|\mathrm{d}T/\mathrm{d}x|\} = 0.36\,\mathrm{mm}$ have been computed adopting the same chemical mechanism (Burke *et al.* 2012); T is the temperature; subscript u or b refers to unburned or burned mixture, respectively.

Case	u'/S_L	$L_{k\varepsilon}/\delta_L$	Da	$(\delta_L/\eta_K)^2$	Δ/η_K	$\Delta/L_{k\varepsilon}$
A	0.7	10.3	11	46	3.0–11.8	0.04–0.17
B	1.9	2.7	1.2	385	8.5–34.0	0.16–0.64

Table 1. Flame characteristics.

The r.m.s. velocity $u' = \sqrt{2\langle k\rangle/3}$, the turbulent kinetic energy $\langle k\rangle = \langle u_k'u_k'\rangle/2$, its dissipation rate $\langle\varepsilon\rangle = 2\nu_u\langle S_{jk}S_{jk}\rangle$, the integral length scale $L_{k\varepsilon} = \langle k\rangle^{3/2}/\langle\varepsilon\rangle$, Damköhler number $Da = L_{k\varepsilon}S_L/(u'\delta_L)$, and the Kolmogorov length scale $\eta_K = (\nu_u^3/\langle\varepsilon\rangle)^{1/4}$ are obtained by averaging over the transverse plane where the plane-averaged fuel-based combustion progress variable $\langle c\rangle(x,t) = 0.05$, followed by time-averaging; $u_k'(\boldsymbol{x},t)$ designates fluctuation of the kth component of the local velocity vector; $S_{jk} = (\partial u_j/\partial x_k + \partial u_k/\partial x_j)/2$ is the rate-of-strain tensor; $\langle q\rangle$ designates time- and transverse-averaged value of the quantity q; and summation convention applies to repeated indexes.

The velocity field $\boldsymbol{u}(\boldsymbol{x},t)$ yielded by the DNS is decomposed into solenoidal and potential components, $\boldsymbol{u}_s(\boldsymbol{x},t)$ and $\boldsymbol{u}_p(\boldsymbol{x},t)$, respectively, adopting numerical methods applied earlier to velocity fields obtained from weakly turbulent single-step chemistry flames (Sabelnikov *et al.* 2021*a*,*b*) and from the two present flames A and B (Sabelnikov *et al.* 2022*a*,*b*). The methods are discussed in detail elsewhere (Sabelnikov *et al.* 2021*a*, 2022*a*). Solenoidal and potential SGS scalar fluxes and inter-scale fluxes were evaluated as follows:

$$\tilde{\boldsymbol{f}}_s = \widetilde{\boldsymbol{u}_s c} - \tilde{\boldsymbol{u}}_s\tilde{c}; \quad \tilde{\boldsymbol{f}}_p = \widetilde{\boldsymbol{u}_p c} - \tilde{\boldsymbol{u}}_p\tilde{c}; \quad G_s = -2\bar{\rho}\widetilde{\boldsymbol{f}}_s\cdot\nabla\tilde{c}; \quad G_p = -2\bar{\rho}\widetilde{\boldsymbol{f}}_p\cdot\nabla\tilde{c}. \tag{3.1a–d}$$

Since all these equations are linear with respect to velocity, $\boldsymbol{f} = \boldsymbol{f}_s + \boldsymbol{f}_p$ and $G = G_s + G_p$.

The computed fields of $\rho(\boldsymbol{x},t)$, $c(\boldsymbol{x},t)$, $\boldsymbol{u}(\boldsymbol{x},t)$, $\boldsymbol{u}_s(\boldsymbol{x},t)$ and $\boldsymbol{u}_p(\boldsymbol{x},t)$, sampled by processing six snapshots ($t/t_e = 0.57$, 0.67, 0.77, 0.86, 0.96 and 1.05 in case A or $t/t_e = 4.1$, 4.8, 5.5, 6.2, 6.8 and 7.5 in case B, where $t_e = L_T/u_0'$) were filtered adopting top-hat (box) filters of three different sizes $\Delta/\delta_L = 0.43$, 0.87 and 1.74, with mass-weighted (Favre) filtering being applied to all these quantities with the exception of density. The smallest and largest filter widths, normalized using η_K or $L_{k\varepsilon}$, are reported in table 1. The combustion progress variable was evaluated using fuel mass fraction Y_F, i.e. $c = (Y_F - Y_{f,u})/(Y_{f,b} - Y_{f,u})$. Quantities conditioned to the normalized filtered dilatation $\Theta = \delta_L\nabla\cdot\tilde{\boldsymbol{u}}/(\tau S_L)$ were sampled by dividing an interval of $\Theta\in[-0.2, 1.3]$ in 100 bins from the entire computational domain and at all instants. Here, $\tau = (\rho_u/\rho_b) - 1$. Probability density functions (PDFs) for various quantities were also sampled using 100 bins from the entire computational domain and at all instants.

4. Results and discussion

Figure 1 shows that time- and transverse-averaged inter-scale flux $\langle G\rangle(x)$ (see black solid lines) is negative for different filters in both flames, i.e. backscatter of SGS scalar variance is well pronounced in each studied case. Even the transverse-averaged counterpart of the filtered $\langle G\rangle$ is negative under the present DNS conditions (not shown for brevity). The backscatter magnitude $|\langle G\rangle|(x)$ and the magnitude of SGS scalar flux (see figure 3, which will be discussed later) peak in the middle of the flame brush, where the probability of

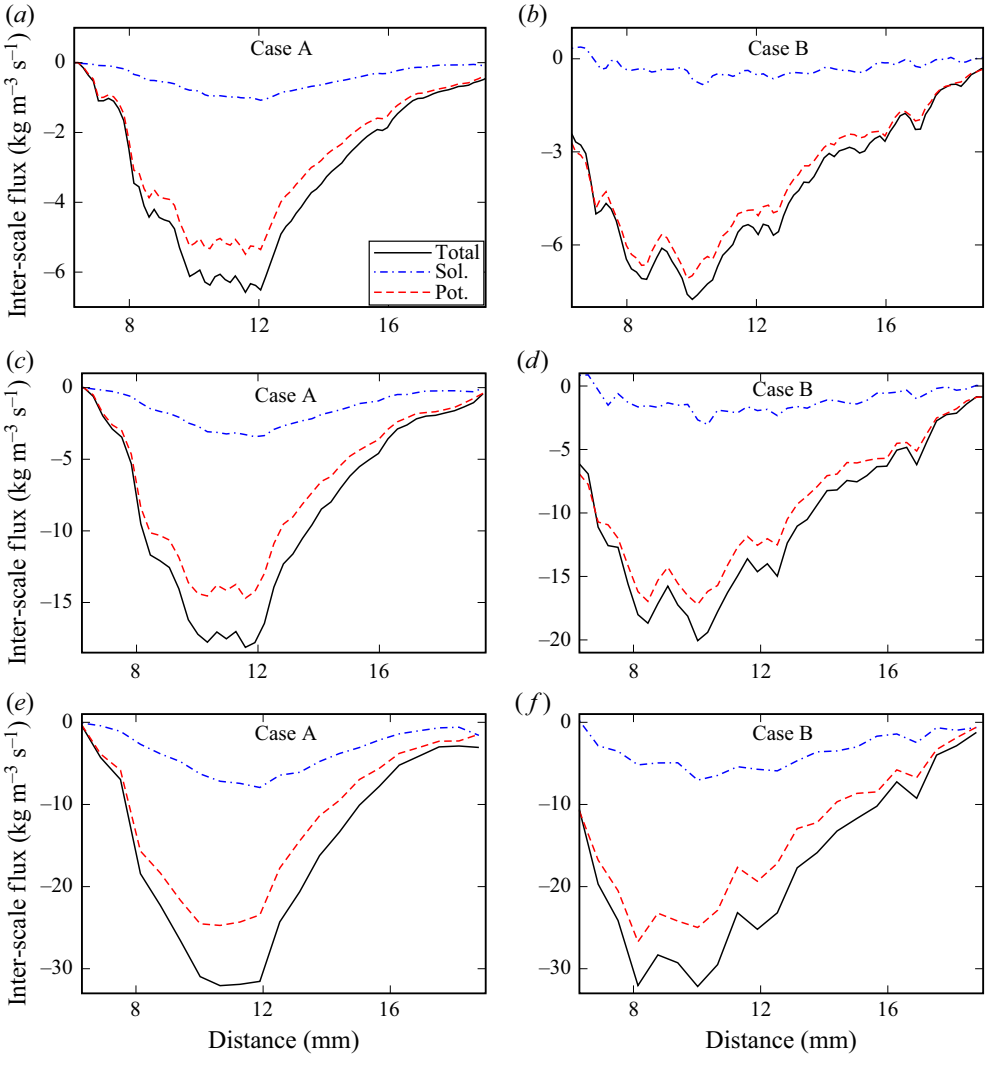

Figure 1. Spatial variations of time- and transverse-averaged inter-scale flux $\langle G\rangle/2$ (black solid lines), as well as solenoidal ($\langle G_s\rangle/2$, blue dotted-dashed lines) and potential ($\langle G_p\rangle/2$, red dashed lines) contributions to it, filtered using a box with sides equal to (a,b) $\Delta = 0.43\delta_L$, (c,d) $\Delta = 0.87\delta_L$ or (e,f) $\Delta = 1.74\delta_L$. Results obtained from flames A and B are shown in the (a,c,e) and (b,d,f), respectively.

finding thin instantaneous flames is the highest and these flames contribute the most to filtered values of quantities that vanish in reactants and products (e.g. ∇c). Moreover, the backscatter magnitude is increased with increasing Δ, because the use of a narrower filter results in decreasing subgrid fluctuations and, in particular, $|\widetilde{\boldsymbol{f}}|$ and $|G|$ (these fluctuations and fluxes vanish at $\Delta \to 0$). With the exception of this trend, results computed using various Δ are similar. For brevity, we will report results obtained adopting the median filter $\Delta = 0.87\delta_L$ in the following.

In figure 1, the backscatter magnitude appears to be almost the same in cases A and B, i.e. depends weakly on u'/S_L or Da. This apparently surprising result could stem, at least in part, from the fact that a ratio of Δ/η_K is higher in more intense turbulence (case B) if the same Δ/δ_L is set in both cases A and B. Due to a higher Δ/η_K, subfilter fluctuations,

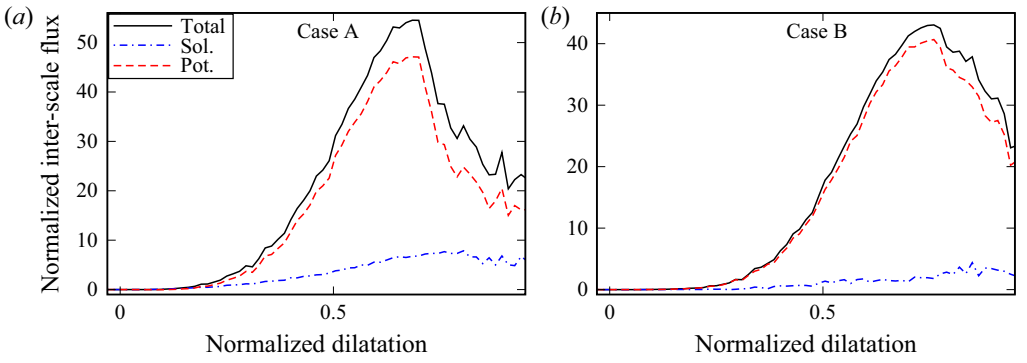

Figure 2. Normalized inter-scale flux $\delta_L\bar{\rho}\tilde{\boldsymbol{f}}\cdot\nabla\tilde{c}/(\rho_u S_L)$ (black solid lines), as well as solenoidal ($\delta_L\bar{\rho}\tilde{\boldsymbol{f}}_s\cdot\nabla\tilde{c}/(\rho_u S_L)$, blue dotted-dashed lines) and potential ($\delta_L\bar{\rho}\tilde{\boldsymbol{f}}_p\cdot\nabla\tilde{c}/(\rho_u S_L)$, red dashed lines) contributions to it, conditioned to normalized filtered dilatation Θ in flames (*a*) A and (*b*) B. $\Delta = 0.87\delta_L$.

$|\tilde{\boldsymbol{f}}|$ and $|G|$ are expected to be larger in flame B, but this is not observed, thus, implying a decrease in backscatter magnitude in more intense turbulence (case B). Indeed, to analyse results obtained using the same Δ/η_K in the two cases, figure 1(*b*) ($\Delta/\eta_K = 8.5$) should be compared with a figure that shows averages of curves plotted in figures 1(*c*) ($\Delta/\eta_K = 5.9$) and 1(*e*) ($\Delta/\eta_K = 11.8$). Such a comparison does indicate a larger $|\langle G\rangle|$ in case A (for the same Δ/η_K), i.e. a decrease in backscatter magnitude with increasing u'/S_L and decreasing Da, in line with DNS data that show mitigation of thermal expansion effects on turbulence at high u'/S_L and low Da, as reviewed by Sabelnikov & Lipatnikov (2017).

While not only the potential $\langle G_p\rangle$ (red dashed lines), but also the solenoidal $\langle G_s\rangle$ (blue dotted-dashed lines) are negative, $|\langle G_p\rangle| \gg |\langle G_s\rangle|$ and $\langle G\rangle$ is mainly controlled by $\langle G_p\rangle$. These results indicate a link between backscatter and potential velocity perturbations, which are not divergence-free, i.e. $\nabla\cdot\boldsymbol{u}_p \neq 0$. Such a link between backscatter and dilatation is further emphasized in figure 2, which shows that, in volumes characterized by significant filtered dilatation, inter-scale fluxes $\bar{\rho}\tilde{\boldsymbol{f}}\cdot\nabla\tilde{c}$ and $\bar{\rho}\tilde{\boldsymbol{f}}_p\cdot\nabla\tilde{c}$ computed for the total and potential velocity fields, respectively, are large and close to one another. On the contrary, the solenoidal flux $\bar{\rho}\tilde{\boldsymbol{f}}_s\cdot\nabla\tilde{c}$ is significantly smaller in such volumes and all three fluxes are very small in volumes characterized by a low dilatation.

Results plotted in figures 1 and 2 suggest the following physical scenario. Combustion-induced heat release and density drop in instantaneous flames cause the local positive dilatation, thus, injecting kinetic energy into turbulent flow, with the injected energy fluctuating in space and time due to fluctuations in the flame orientation (the local flow accelerates along the normal to the flame). Since solenoidal velocity field is divergence-free, the dilatation causes potential velocity fluctuations. Even if the injection-zone volume (i.e. volume occupied by the flames) is significantly less than the mean flame brush volume, the injected kinetic energy can be statistically significant (Sabelnikov *et al.* 2022*a*,*b*) due to high local energy-injection rates controlled by the local dilatation. Moreover, the scalar c is injected into the scalar field within such flames due to the local formation of combustion products. Thus, extra turbulent energy (potential) and extra scalar energy c^2 are injected at small scales of the order of δ_L, with these injections inverting cascade for the scalar c. Indeed, since the local potential flow accelerates from unburned ($c = 0$) to burned ($c = 1$) flame edges, correlation between the local potential velocity and c is positive (in the coordinate framework adopted here) within flames and the potential flux $\tilde{\boldsymbol{f}}_p$ is predominantly positive (i.e. counter-gradient), thus, making the potential inter-scale flux G_p predominantly negative (if the filter contains a flame zone

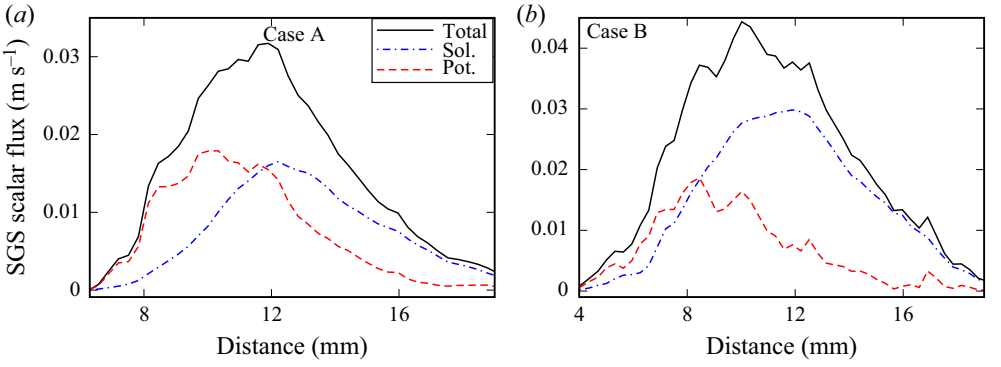

Figure 3. Spatial variations of time- and transverse-averaged axial SGS scalar flux $\langle\tilde{f}_x\rangle$ (black solid lines), as well as solenoidal ($\langle\tilde{f}_{x,s}\rangle$, blue dotted-dashed lines) and potential ($\langle\tilde{f}_{x,p}\rangle$, red dashed lines) contributions to it obtained from flames (*a*) A and (*b*) B and filtered using a box with sides equal to $\Delta = 0.87\delta_L$.

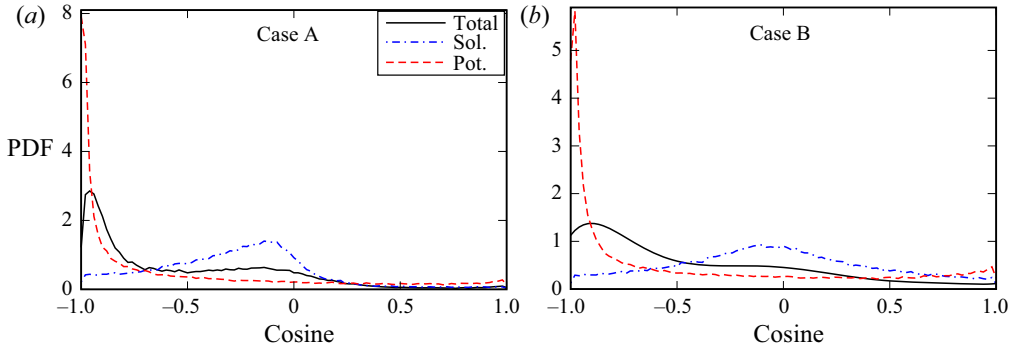

Figure 4. Probability density functions for cosine between vectors $\tilde{\boldsymbol{f}}$ and $\boldsymbol{\nabla}\tilde{c}$ sampled from volumes where $0.05 \leq \tilde{c}(\boldsymbol{x}, t) \leq 0.95$ in flames (*a*) A and (*b*) B. $\Delta = 0.87\delta_L$. Legends are explained in the caption of figure 3.

inside it). Appearance of the counter-gradient potential scalar flux $\tilde{\boldsymbol{f}}_p$ is confirmed in figure 3 (red dashed lines).

Comparison of figures 1 and 3 shows two interesting features. First, in the latter figure, magnitudes of $\langle\tilde{f}_{x,s}\rangle$ and $\langle\tilde{f}_{x,p}\rangle$ are comparable in flame A and the solenoidal flux $\langle\tilde{f}_{x,s}\rangle$ is even larger than the potential $\langle\tilde{f}_{x,p}\rangle$ in flame B, whereas $|\langle G_p\rangle| \gg |\langle G_s\rangle|$ in both flames (figure 1). This difference between contributions of potential flow to scalar and inter-scale fluxes stems from the fact that the vector $\tilde{\boldsymbol{f}}_p$ ($\tilde{\boldsymbol{f}}_s$) is more (less) collinear with $\boldsymbol{\nabla}\tilde{c}$ (figure 4). The preferential alignment of $\tilde{\boldsymbol{f}}_p$ and $\boldsymbol{\nabla}\tilde{c}$ is associated with the facts that (i) dilatation and potential velocity are directly linked, whereas $\boldsymbol{\nabla}\cdot\boldsymbol{u}_s = 0$, and (ii) dilatation in a local flame stems from velocity variations along the local normal to the flame, i.e. along the direction of the vector $\boldsymbol{\nabla}c$. The highlighted link of dilatation with the local alignment of the vectors $\tilde{\boldsymbol{f}}_p$ and $\boldsymbol{\nabla}\tilde{c}$ is further supported in figure 5, which shows that the two vectors are almost collinear if $\Theta = \delta_L\boldsymbol{\nabla}\cdot\boldsymbol{u}/(\tau S_L) > 0.5$ (note that the figure shows $-\tilde{\boldsymbol{f}}_p$). This trend is more pronounced in case A characterized by a lower u'/S_L and a higher Da.

Second, even the solenoidal scalar flux $\tilde{\boldsymbol{f}}_s$ shows the counter-gradient behaviour under conditions of the present study (blue dotted-dashed lines in figure 3), thus, making the solenoidal inter-scale flux G_s predominantly negative also. However, this phenomenon

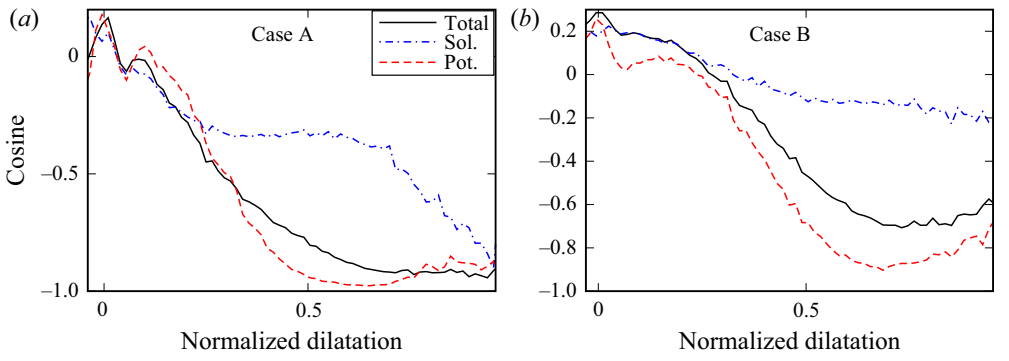

Figure 5. Cosine between vectors $-\tilde{\boldsymbol{f}}$ and $\nabla\tilde{c}$ conditioned to normalized filtered dilatation Θ in flames (*a*) A and (*b*) B. $\Delta = 0.87\delta_L$. Legends are explained in the caption of figure 3.

contributes little to total backscatter ($|\langle G_p\rangle| \gg |\langle G_s\rangle|$ in figure 1 due to poor alignment of the vectors $\tilde{\boldsymbol{f}}_s$ and $\nabla\tilde{c}$ (blue dotted-dashed lines in figures 4 and 5)). Due to a minor contribution of this phenomenon to scalar backscatter, the counter-gradient behaviour of the solenoidal scalar flux is beyond the scope of the present communication. Briefly speaking, the phenomenon results from the smoothing of the flame surface by vorticity generated by baroclinic torque within flames. The reader interested in a more detail discussion is referred to recent studies of a similar phenomenon within RANS framework (Lipatnikov *et al.* 2018, 2019; Sabelnikov *et al.* 2021*b*, 2022*b*).

5. Concluding remarks

By analysing complex-chemistry DNS data obtained earlier from lean hydrogen–air flames, backscatter of SGS scalar variance is documented not only in weakly turbulent flame A, but also in flame B associated with moderately intense small-scale turbulence and characterized by a unity-order Damköhler number and a ratio of Kolmogorov length scale to thermal laminar flame thickness as low as 0.05.

Application of HHD to the velocity fields yielded by the DNS, followed by an analysis of the obtained solenoidal and potential velocity fields, have shown that the documented backscatter stems primarily from the potential velocity perturbations generated due to dilatation in instantaneous local flames. The backscatter is substantially promoted by a close alignment of the spatial gradient of filtered scalar $\tilde{c}$ and the potential-velocity contribution to the local SGS scalar flux. The alignment is associated with the fact that combustion-induced thermal expansion increases local velocity in the direction of ∇c.

Decomposition of a velocity field into potential (dilatational) and solenoidal (rotational) components is an essential step towards exploring the influence of combustion on cascades of turbulent kinetic energy and mixture non-uniformities.

The above findings call for further development of SGS models of the inter-scale flux $\bar{\rho}\tilde{\boldsymbol{f}}\cdot\nabla\tilde{c}$ of scalar variance for LES of premixed turbulent combustion.

Acknowledgements. Computational resources for the DNS were provided by the KAUST Supercomputing Laboratory. Valuable comments by the referees are gratefully acknowledged.

Funding. V.A.S. gratefully acknowledges the financial support by ONERA and by the Grant of the Ministry of Science and Higher Education of the Russian Federation (Grant agreement of December 8, 2020 No. 075-11-2020-023) within the program for the creation and development of the World-Class Research Center 'Supersonic' for 2020–2025. A.N.L. gratefully acknowledges the financial support by Chalmers Area

of Advance Transport. F.E.H.P. and H.G.I. were sponsored by King Abdullah University of Science and Technology (KAUST).

Declaration of interests. The authors report no conflict of interest.

Author ORCIDs.
V.A. Sabelnikov https://orcid.org/0000-0002-0979-2994;
A.N. Lipatnikov https://orcid.org/0000-0001-5682-4947;
N.V. Nikitin https://orcid.org/0000-0003-2284-5218;
H.G. Im https://orcid.org/0000-0001-7080-1266.

References

Ahmed, U., Chakraborty, N. & Klein, M. 2019 On the stress-strain alignment in premixed turbulent flames. *Sci. Rep.* **9**, 5092.

Alexakis, A. & Biferale, L. 2018 Cascades and transitions in turbulent flows. *Phys. Rep.* **767–769**, 1–101.

Bilger, R.W., Pope, S.B., Bray, K.N.C. & Driscoll, J.F. 2005 Paradigms in turbulent combustion research. *Proc. Combust. Inst.* **30**, 21–42.

Boger, M., Veynante, D., Boughanem, H. & Trouve, A. 1998 A direct numerical simulation analysis of flame surface density concept for large eddy simulation of turbulent premixed combustion. *Proc. Combust. Inst.* **27**, 917–925.

Borue, V. & Orszag, S.A. 1998 Local energy flux and subgrid-scale statistics in three-dimensional turbulence. *J. Fluid Mech.* **366**, 1–31.

Burke, P., Chaos, M., Ju, Y., Dryer, F.L. & Klippenstein, S.J. 2012 Comprehensive H_2/O_2 kinetic model for high–pressure combustion. *Intl J. Chem. Kinet.* **44**, 444–474.

Cerutti, S. & Meneveau, C. 1998 Intermittency and relative scaling of subgrid-scale energy dissipation in isotropic turbulence. *Phys. Fluids* **10**, 928–937.

Chen, J.H. & Im, H.G. 2000 Stretch effects on the burning velocity of turbulent premixed hydrogen-air flames. *Proc. Combust. Inst.* **28**, 211–218.

Chertkov, M., Kolokolov, I. & Vergassola, M. 1998 Inverse versus direct cascades in turbulent advection. *Phys. Rev. Lett.* **80**, 512–515.

Chorin, A.J. & Marsden, J.E. 1993 *A Mathematical Introduction to Fluid Mechanics*. Springer.

Damköhler, G. 1940 Der einfuss der turbulenz auf die flammengeschwindigkeit in gasgemischen. *Z. Electrochem.* **46**, 601–652.

Datta, A., Mathew, J. & Hemchandra, S. 2022 The explicit filtering method for large eddy simulations of a turbulent premixed flame. *Combust. Flame* **237**, 111862.

Frisch, U. 1995 *Turbulence. The Legacy of A.N. Kolmogorov*. Cambridge University Press.

Gawedzki, K. & Vergassola, M. 2000 Phase transition in the passive scalar advection. *Physica* D **138**, 63–90.

Im, H.G., Arias, P.G., Chaudhuri, S. & Uranakara, H.A. 2016 Direct numerical simulations of statistically stationary turbulent premixed flames. *Combust. Sci. Technol.* **188**, 1182–1198.

Im, H.G. & Chen, J.H. 2002 Preferential diffusion effects on the burning rate of interacting turbulent premixed hydrogen-air flames. *Combust. Flame* **131**, 246–258.

Jiménez, C., Valiño, L. & Dopazo, C. 2001 A priori and a posteriori tests of subgrid scale models for scalar transport. *Phys. Fluids* **13**, 2433–2436.

Kazbekov, A. & Steinberg, A. 2021 Physical space analysis of cross-scale turbulent kinetic energy transfer in premixed swirl flames. *Combust. Flame* **229**, 111403.

Kazbekov, A. & Steinberg, A. 2023 Influence of flow structure and combustion on cross-scale turbulent kinetic energy transfer in premixed swirl flames. *Proc. Combust. Inst.* **39** (in press).

Kim, J., Bassenne, M., Towery, C.A.Z., Hamlington, P.E., Poludnenko, A.Y. & Urzay, J. 2018 The cross-scale physical-space transfer of kinetic energy in turbulent premixed flames. *J. Fluid Mech.* **848**, 78–116.

Klein, M., Chakraborty, N. & Gao, Y. 2016 Scale similarity based models and their application to subgrid scale scalar flux modelling in the context of turbulent premixed flames. *Intl J. Heat Fluid Flow* **57**, 91–108.

Klein, M., Herbert, A., Kosaka, H., Böhm, B., Dreizler, A., Chakraborty, N., Papapostolou, V., Im, H.G. & Hasslberger, J. 2020 Evaluation of flame area based on detailed chemistry DNS of premixed turbulent hydrogen-air flames in different regimes of combustion. *Flow Turbul. Combust.* **104**, 403–419.

KLEIN, M., KASTEN, C., CHAKRABORTY, N., MUKHADIYEV, N. & IM, H.G. 2018 Turbulent scalar fluxes in H_2-air premixed flames at low and high Karlovitz numbers. *Combust. Theor. Model.* **22**, 1033–1048.

KOBAYASHI, H. 2005 The subgrid-scale models based on coherent structures for rotating homogeneous turbulence and turbulent channel flow. *Phys. Fluids* **17**, 045104.

KOLLA, H., HAWKES, E.R., KERSTEIN, A.R., SWAMINATHAN, N. & CHEN, J.H. 2014 On velocity and reactive scalar spectra in turbulent premixed flames. *J. Fluid Mech.* **754**, 456–487.

KOLMOGOROV, A.N. 1941 The local structure of turbulence in incompressible viscous fluid for very large Reynolds number. *Dokl. Akad. Nauk SSSR* **30**, 299–303.

LECOCQ, G., RICHARD, S., COLIN, O. & VERVISCH, L. 2010 Gradient and counter-gradient modeling in premixed flames: theoretical study and application to the LES of a lean premixed turbulent swirl-burner. *Combust. Sci. Technol.* **182**, 465–479.

LESIEUR, M., METAIS, O. & COMTE, P. 2005 *Large-Eddy Simulations of Turbulence*. Cambridge University Press.

LESLIE, D.C. & QUARINI, G.L. 1979 The application of turbulence theory to the formulation of subgrid modelling procedures. *J. Fluid Mech.* **91**, 65–91.

LIPATNIKOV, A.N. & CHOMIAK, J. 2005 Molecular transport effects on turbulent flame propagation and structure. *Prog. Energy Combust. Sci.* **31**, 1–73.

LIPATNIKOV, A.N., SABELNIKOV, V.A., HERNÁNDEZ-PÉREZ, F.E., SONG, W. & IM, H.G. 2020 A priori DNS study of applicability of flamelet concept to predicting mean concentrations of species in turbulent premixed flames at various Karlovitz numbers. *Combust. Flame* **222**, 370–382.

LIPATNIKOV, A.N., SABELNIKOV, V.A., HERNÁNDEZ-PÉREZ, F.E., SONG, W. & IM, H.G. 2021 Prediction of mean radical concentrations in lean hydrogen-air turbulent flames at different Karlovitz numbers adopting a newly extended flamelet-based presumed PDF. *Combust. Flame* **226**, 248–259.

LIPATNIKOV, A.N., SABELNIKOV, V.A., NISHIKI, S. & HASEGAWA, T. 2018 Does flame-generated vorticity increase turbulent burning velocity? *Phys. Fluids* **30**, 081702.

LIPATNIKOV, A.N., SABELNIKOV, V.A., NISHIKI, S. & HASEGAWA, T. 2019 A direct numerical simulation study of the influence of flame-generated vorticity on reaction-zone-surface area in weakly turbulent premixed combustion. *Phys. Fluids* **31**, 055101.

MACART, J.F. & MUELLER, M.E. 2021 Damköhler number scaling of active cascade effects in turbulent premixed combustion. *Phys. Fluids* **33**, 035103.

MANIAS, D.M., TINGAS, E.A., HERNÁNDEZ PÉREZ, F.E., GALASSI, R.M., CIOTTOLI, P.P., VALORANI, M. & IM, H.G. 2019 Investigation of the turbulent flame structure and topology at different Karlovitz numbers using the tangential stretching rate index. *Combust. Flame* **200**, 155–167.

MARSTORP, L., BRETHOUWER, G. & JOHANSSON, A.V. 2007 A stochastic subgrid model with application to turbulent flow and scalar mixing. *Phys. Fluids* **19**, 035107.

MENEVEAU, C. 2000 Scale-invariance and turbulence models for large-eddy simulation. *Annu. Rev. Fluid Mech.* **32**, 1–32.

MONIN, A.S. & YAGLOM, A.M. 1975 *Statistical Fluid Mechanics: Mechanics of Turbulence*, vol. 2. The MIT Press.

O'BRIEN, J., TOWERY, C.A.Z., HAMLINGTON, P.E., IHME, M., POLUDNENKO, A.Y. & URZAY, J. 2017 The cross-scale physical space transfer of kinetic energy in turbulent premixed flames. *Proc. Combust. Inst.* **36**, 1967–1975.

PASSOT, T. & POUQUET, A. 1987 Numerical simulation of compressible homogeneous flows in the turbulent regime. *J. Fluid Mech.* **181**, 441–466.

PFADLER, S., DINKELACKER, F., BEYRAU, F. & LEIPERTZ, A. 2009 High resolution dual-plane stereo-PIV for validation of subgrid scale models in large-eddy simulations of turbulent premixed flames. *Combust. Flame* **156**, 1552–1564.

PIOMELLI, U., CABOT, W.H., MOIN, P. & LEE, S. 1991 Subgrid-scale backscatter in turbulent and transitional flows. *Phys. Fluids* **3**, 1766–1771.

POINSOT, T. & VEYNANTE, D. 2005 *Theoretical and Numerical Combustion*, 2nd edn. Edwards.

QIAN, X., LU, H., ZOU, C. & YAO, H. 2022 On the inverse kinetic energy cascade in premixed isotropic turbulent flames. *Intl J. Mod. Phys.* **33**, 2250015.

RANJAN, R. & MENON, S. 2018 Vorticity, backscatter and counter-gradient transport predictions using two-level simulation of turbulent flows. *J. Turbul.* **19**, 334–364.

RANJAN, R., MURALIDHARAN, B., NAGAOKA, Y. & MENON, S. 2016 Subgrid-scale modeling of reaction-diffusion and scalar transport in turbulent premixed flames. *Combust. Sci. Technol.* **188**, 1496–1537.

RICHARD, S., COLIN, O., VERMOREL, O., BENKENIDA, A., ANGELBERGER, C. & VEYNANTE, D. 2007 Towards large eddy simulation of combustion in spark ignition engines. *Proc. Combust. Inst.* **31**, 3059–3066.

RICHARDSON, L.F. 1922 *Weather Prediction by Numerical Process*. Cambridge University Press.

ROGALLO, R.S. 1981 Numerical experiments in homogeneous turbulence. *NASA Tech. Mem.* 81315, NASA Ames Research Center.

SABELNIKOV, V.A. & LIPATNIKOV, A.N. 2017 Recent advances in understanding of thermal expansion effects in premixed turbulent flames. *Annu. Rev. Fluid Mech.* **49**, 91–117.

SABELNIKOV, V.A. & LIPATNIKOV, A.N. 2021 Scaling of reaction progress variable variance in highly turbulent reaction waves. *Phys. Fluids* **33**, 085103.

SABELNIKOV, V.A., LIPATNIKOV, A.N., NIKITIN, N., HERNÁNDEZ-PÉREZ, F.E. & IM, H.G. 2022*a* Conditioned structure functions in turbulent hydrogen/air flames. *Phys. Fluids* **34**, 085103.

SABELNIKOV, V.A., LIPATNIKOV, A.N., NIKITIN, N., HERNÁNDEZ-PÉREZ, F.E. & IM, H.G. 2022*b* Effects of thermal expansion on moderately intense turbulence in premixed flames. *Phys. Fluids* **34**, 115127.

SABELNIKOV, V.A., LIPATNIKOV, A.N., NIKITIN, N., NISHIKI, S. & HASEGAWA, T. 2021*a* Application of Helmholtz-Hodge decomposition and conditioned structure functions to exploring influence of premixed combustion on turbulence upstream of the flame. *Proc. Combust. Inst.* **38**, 3077–3085.

SABELNIKOV, V.A., LIPATNIKOV, A.N., NIKITIN, N., NISHIKI, S. & HASEGAWA, T. 2021*b* Solenoidal and potential velocity fields in weakly turbulent premixed flames. *Proc. Combust. Inst.* **38**, 3087–3095.

SABELNIKOV, V.A., LIPATNIKOV, A.N., NISHIKI, S., DAVE, H.L., HERNÁNDEZ-PÉREZ, F.E., SONG, W. & IM, H.G. 2021*c* Dissipation and dilatation rates in premixed turbulent flames. *Phys. Fluids* **33**, 035112.

SABELNIKOV, V.A., YU, R. & LIPATNIKOV, A.N. 2019 Thin reaction zones in constant-density turbulent flows at low Damköhler numbers: theory and simulations. *Phys. Fluids* **31**, 055104.

SAGAUT, P. 2006 *Large Eddy Simulation for Incompressible Flows, An Introduction*. Springer.

TOWERY, C.A.Z., POLUDNENKO, A.Y., URZAY, J., O'BRIEN, J., IHME, M. & HAMLINGTON, P.E. 2016 Spectral kinetic energy transfer in turbulent premixed reacting flows. *Phys. Rev.* E **93**, 053115.

TULLIS, S. & CANT, R.S. 2002 Scalar transport modeling in large eddy simulation of turbulent premixed flames. *Proc. Combust. Inst.* **29**, 2097–2104.

URANAKARA, H.A., CHAUDHURI, S., DAVE, H.L., ARIAS, P.G. & IM, H.G. 2016 A flame particle tracking analysis of turbulence-chemistry interaction in hydrogen-air premixed flames. *Combust. Flame* **163**, 220–240.

WACKS, D.H., CHAKRABORTY, N., KLEIN, M., ARIAS, P.G. & IM, H.G. 2016 Flow topologies in different regimes of premixed turbulent combustion: a direct numerical simulation analysis. *Phys. Rev. Fluids* **1**, 083401.

WELLER, H.G., TABOR, G., GOSMAN, A.D. & FUREBY, C. 1998 Application of flame wrinkling LES combustion model to a turbulent mixing layer. *Proc. Combust. Inst.* **27**, 899–907.